Three-dimensional SPH simulation of a twin-fluid atomizer operating at high pressure

G. Chaussonnet[*,1], S. Braun[1], T. Dauch[1], M. Keller[1], J. Kaden[1], T. Jakobs[2], C. Schwitzke[1], R. Koch[1], H.-J. Bauer[1]

Karlsruher Institut für Technologie (KIT), Karlsruhe, Germany
[1]Institut für Thermische Strömungsmaschinen
[2]Institute für Technische Chemie
[*]geoffroy.chaussonnet@kit.edu

Abstract

In the context of biofuel production, a twin-fluid atomizer is investigated by the means of the Weakly-Compressible Smoothed Particle Hydrodynamics (WCSPH) method. This configuration consists of a round liquid jet discharging at low velocity into a quiescent cavity. The liquid is atomized by a high-speed turbulent co-flow. This configuration has been studied experimentally as well. In order to reflect the experimental conditions, the liquid is a mixture of Glycerol and water and a constant viscosity is set to 200 mPa s. The ambient pressure is 11 bar and the gas velocity is 58.3 m/s, leading to a gas Reynolds number of 137 000 and a Weber number of 1375. The three-dimensional numerical domain consists of the twin-fluid nozzle and a cavity of 30 mm length and 17.4 mm diameter. The spatial resolution is 33 µm, which leads to 208 million of particles. The simulation is run for 45 ms of physical time using 2000 CPU. The results show that the fiber-mode breakup is well captured by the method. The shape and the dynamics of the fragmented liquid lumps are in very good qualitative agreement with the experimental observations. Further quantitative analyses are performed in terms of time average of the liquid phase, and time evolution of the spray characteristics at the exit of the cavity. Finally, due to the Lagrangian nature of the SPH method, the breakup sequence of each liquid elements can be monitored and collected. Hence, the fragmentation spectrum of this configuration is also presented.

Keywords: air-assisted atomization, smoothed particle hydrodynamics, spray characteristics, fragmentation spectrum

---

Introduction

In the context of renewable energies, the gasification process allows to transform agricultural waste into liquid fuel [1]. The reaction of gasification occurs in a pressurized reactor where the reactant, a non-Newtonian bio slurry of high viscosity, is injected as spray. The quality of the spray has a strong influence on the overall efficiency of the process [2]. Hence, the design of the nozzle is of primary importance. Gasification takes place at high pressure and temperature (p = 80 bar and T $\approx$ 1500°C), which limits the instrumentation of the gasifier. The numerical simulation is therefore a suitable method for analyzing the breakup process occurring at these operating conditions. Recent numerical simulations of air-assisted atomization at high pressure (resp. at high gas density) using first principles methods are very scarce in the literature [3, 4, 5]. Due to the broad range of time and length scale involved in this process, the converged spray characteristics were never simulated.
In this paper, the Smooth Particle Hydrodynamics (SPH) method is employed [6]. It is a mesh-free method that relies on a Lagrangian description, where the discretization points (called *particles*) move at the fluid velocity. The physical properties (mass, momentum and energy) are attributed to each particle. Thus, the advection is naturally handled by the particle motion and is not prone to numerical diffusion. This is also an advantage when capturing the phase interface in the case of multiphase flow: no surface reconstruction algorithm is needed. The SPH method applied to air-assisted liquid breakup was pioneered by Höfler *et al.* [7] and is now successfully applied to different configurations of fuel injectors [8, 9]. It is shown is the present paper that SPH allows to access information on the breakup process, which is not easily feasible in mesh-based methods.
After this introduction, the reference experiment is presented, followed by a brief description of the SPH method. Then, the setup used for the numerical computation is described. The rest of the paper covers a discussion of the results, with qualitative comparison with the experiment.

Reference experiment

The reference experiment consists of a twin-fluid external mixing nozzle as depicted in Fig. 1 (left) that discharges in a pressurized cavity [10, 11]. The liquid is injected at low velocity as cylindrical jet, and the gas is injected in a coaxial high-speed annular stream enclosing the liquid. The liquid duct diameter D_l, the height H_g

of the annular gas duct, the separator thickness e_s and the outer diameter D_g of the gas duct are 2, 1.6, 0.1 and $5.4\,\mathrm{mm}$, respectively. The liquid is a mix of Glycerol and water. Its characteristics are a density ρ_l of 1233 kg/m^3, a constant dynamic viscosity μ_l of 0.2 Pa s, and a surface tension σ of 63.6 N/m. The vessel is pressurized to 11 bar and the temperature is kept to 20°C, resulting into a density ρ_g of 13.25 kg/m^3 and a dynamic viscosity μ_g of 18.61 µPa s. The mean gas velocity is $58\,\mathrm{m/s}$. The non-dimensional numbers that characterize this experiment are:

$$\mathrm{Re} = \frac{\rho D_h U}{\mu},\ \mathrm{We} = \frac{\rho_g D_l U_{rel}^2}{\sigma},\ \mathrm{Oh} = \frac{\mu_l}{\sqrt{\sigma\,\rho_l\,D_l}} \tag{1}$$

Equations (1) refer to, in order of appearance: the Reynolds number where D_h is the hydraulic diameter equal to D_l for the liquid and $2H_g$ for the gas, the Weber number where U_{rel} is the liquid/gas relative velocity, and the Ohnesorge number. Their values are Re_g=137000, We=1375 and Oh=0.048. Additionally, two operating parameters are introduced in this type of geometry. The gas-to-liquid mass ratio (GLR) and the momentum flux ratio M:

$$\mathrm{GLR} = \frac{\dot{m}_g}{\dot{m}_l} \quad \text{and} \quad \mathrm{M} = \frac{\rho_g U_g^2}{\rho_l U_l^2} \tag{2}$$

and are equal to 4.4 and 49, respectively. They correspond to a gas and liquid mass flow rate of 14.8 and 3.3 g/s.

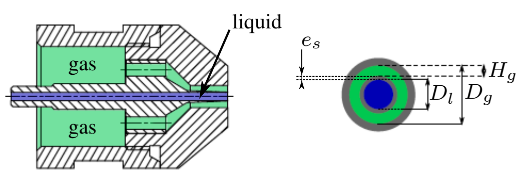

Figure 1 Schematics of external mixing twin fluid atomizer, side view (*left*) and front view (*right*).

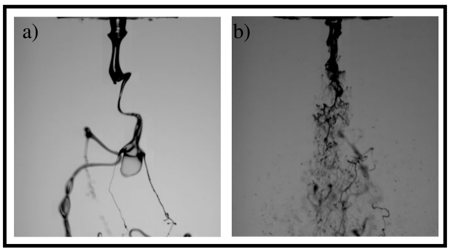

Figure 2 Membrane-breakup (a) at 1 bar (GLR = 0.36) and fiber-breakup (b) at 7 bar (GLR = 2.5), from [11]

In the experiment, the liquid disintegration was recorded by a high-speed camera. The ambient pressure was found to have a major impact on the type of breakup regime. At lower ambient pressure, the liquid is disrupted in a *membrane* mode (Fig. 2a), where the liquid forms thin membranes in a similar way like the bag breakup. When the pressure is increased, the *fiber*-type breakup occurs. It is characterized by the presence of smaller stretched lumps (Fig. 2b). The regime corresponding to the operating conditions studied in the present simulation is the fiber-type breakup.

Numerical Model

Smoothed Particles Hydrodynamics method

In the SPH mehod, the physical quantities and their gradient at a particle location (a) are determined by the interpolation over the values of its neighbors (b) according to [6]:

$$f(\boldsymbol{r}_a) = \sum_{b\in\Omega_a} V_b\, f(\boldsymbol{r}_b)\, W(\boldsymbol{r}_b - \boldsymbol{r}_a, h) \tag{3}$$

where V_b is the volume of the adjacent particles. The term W is a weighting function (the *kernel*). It depends on the inter particle distance $\boldsymbol{r}_b - \boldsymbol{r}_a$ and a characteristic length scale h called the *smoothing length*. The kernel promotes the influence of closer neighbors as illustrated in 2D in Fig. 3 (*top*). When the neighbors are located outside the *sphere of influence* of the central particle (Fig. 3 *bottom*), they are not taken into account. Hence, the kernel has a compact support.

In the present study, two isothermal weakly-compressible non-miscible fluids are considered. In the Navier-Stokes equations the source terms in the momentum equation are the pressure gradient, the viscous term proportional to the Laplacian of the velocity, the surface tension force and the gravity. No evaporation is taken into account. These equations are formulated in a Lagrangian frame of reference and solved using the SPH method. The interested reader is referred to [9] for further details about the modeling.

Numerical Setup

The numerical domain, as depicted in Figs. 4 and 5, is simplified. It contains the nozzle and just a fraction of the reactor, in order to reduce the computational effort. The pressurized cavity of the experiment is reduced in

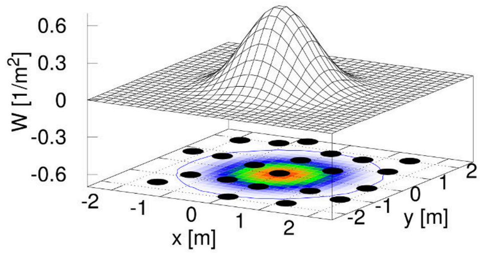

Figure 3 Top part: Surface of a 2-D kernel. Bottom part: Particle distribution superimposed with the kernel color map and illustration of the sphere of influence.

the simulation to the cylindrical region in the vicinity of the nozzle, covering an axial distance of 30 mm from the nozzle exit and a radius R_c of 8.7 mm. The trajectory of the spray droplets might be influenced by this confined domain, but the fundamental process of atomization will not be affected. The length of the gas channel is 6 H_g and that of the liquid channel is only D_l long due to the low Reynolds number Re_l. A turbulent and a laminar profile are set at the gas and liquid channel inlet, respectively. The wall of the outer crown of the nozzle is limited to 3 mm. On the walls of the nozzle a no-slip boundary condition is imposed. An additional gas inlet of 3 mm height is added on the outer radius of the cavity to take into account the entrainment of air caused by the coaxial jet. The entrainment velocity is set to 14.84 m/s. It ensures an appropriate entrainment rate up to the outlet of the cavity [12]. On the side of the cavity a wall without friction is imposed. Finally, at the outlet a constant pressure of 11 bar is set. Figure 5 shows the slices where the spray characteristics will be determined.

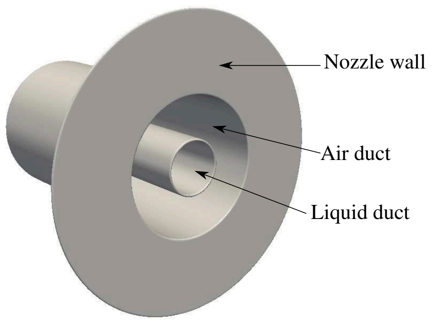

Figure 4 Close-up view of the nozzle, superimposed with the virtual rings.

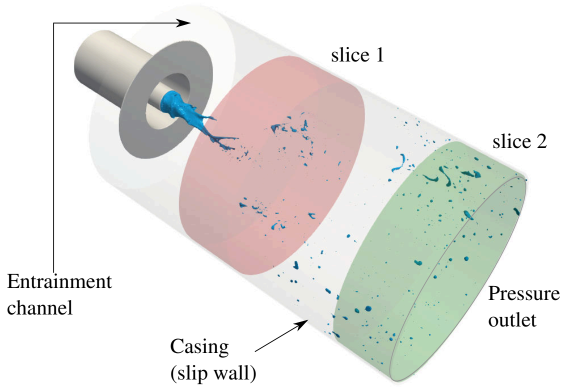

Figure 5 Numerical domain superimposed with the virtual slices.

At the initiation of the simulation, the cavity is filled with gas particles and the liquid jet is initialized as a 5 mm long cylinder. The initial inter-particle spacing is equal to 33.33 µm, which leads to 208 million inner particles and 370 thousand boundary markers. Markers are special stationary particles located at the inlet and outlet boundaries of the domain. They are used to impose the boundary conditions. The simulation is run on 2000 cores for a physical time of 45 ms. This is equivalent to 87 flow-through times of the gas. The initialization of the liquid jet is obtained after 6 ms, which leads to 39 ms (76 convective times) of physical time to collect statistics on the spray. With a mean time step Δt of 28 ns, the simulation is run over 1.6 million time iterations. This amounts to a total computational cost of 1.2 millions CPU-hours. In total 1553 time steps were saved, corresponding to a sampling frequency of 34.5 kHz. The data of each saved time step has a total size of 11.69 Go.

Qualitative results

The results of the simulation is qualitatively compared to the high-speed images of the experiment in Fig. 6. The simulation captures well the flapping of the jet that occurs intermittently in the experiment, and which is characterized by a shape of a hook. Please note that this flapping motion occurs in the fiber-type breakup and therefore it does not correspond strictly to a flapping instability, which is related to a membrane-type breakup. The agreement is good, both in terms of the length scales as well as the temporal evolution of the hook shape. However, the spray shows a lower volume fraction in the simulation, especially at the tip of the liquid jet. This discrepancy can be attributed to the fact that (i) more liquid is contained in the tip of the jet in the experiment, (ii) in the simulation liquid droplets containing less than five numerical particles were dismissed, leading to a significant overall reduction of the spray volume and (iii) the surface smoothing procedure used for post-process causes a reduction of the volume of the liquid.

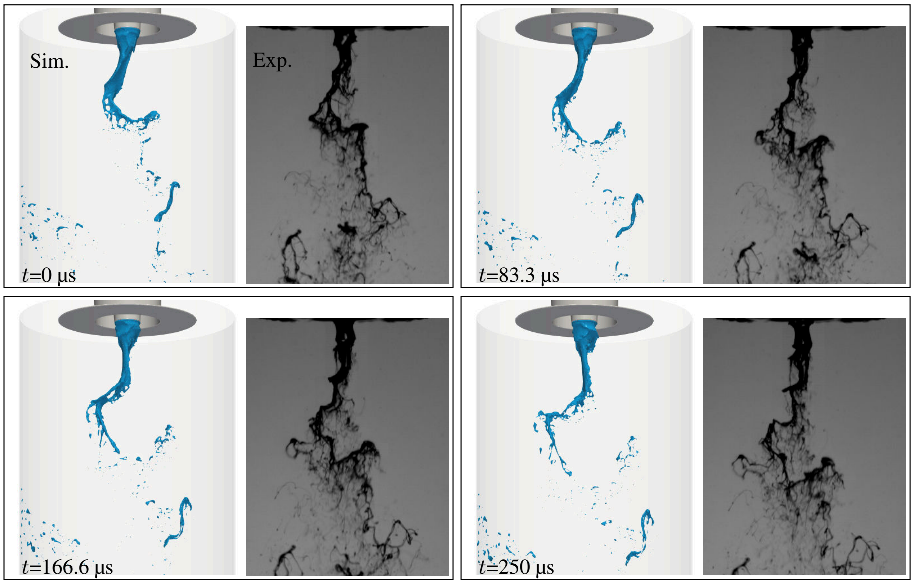

Figure 6 Time series of the simulation and the experiment.

Quantitative results

For analyzing the spray characteristics, a Connected Component Labeling [13] technique was applied. This technique allows to identify each cluster of numerical particles as a continuous liquid lump. A cluster is defined as a connected volume made of liquid particles where the maximum distance between two consecutive particles is $3\,dx$. The position, the velocity and the volume of each cluster is calculated from the corresponding values of its numerical particles, and the diameter of equivalent spherical volume can be calculated. In addition, the sphericity φ of the cluster was determined. These quantities can be used directly in their Lagrangian form or they can be projected on a mesh to be time-averaged and to give access to the liquid volume concentration. It is emphasized that in the present study, clusters that contain less than 5 particles are dismissed due to too coarse spatial resolution. This is equivalent to dismissing droplets smaller than $2\,dx$.

Axial evolution of time-averaged liquid quantities

The numerical particles of the *liquid* type were projected on the center axis with coordinate z to obtain axial profiles. This projection corresponds to averaging the particle quantities inside a slice of volume $\mathrm{d}V(z) = 2\pi R_c\,\mathrm{d}z$. For instance, the mean liquid fraction α_l at the location z is given by:

$$\alpha_l(z) = \frac{1}{\mathrm{d}V(z)}\frac{1}{t_f - t_0}\int_{t=t_0}^{t_f}\left(\sum_{p\in dV(z)} V_p\right)\mathrm{d}t \tag{4}$$

where V_p is the particle volume. The axial profiles of the liquid fraction α_l, the droplet concentration N_d, the Sauter Mean Diameter (SMD) and the sphericity φ are depicted in Fig. 7. Liquid lumps with an equivalent diameter larger than 2 mm were discarded because they correspond to a portion of the central liquid jet that was just detached from the main core. Therefore these liquid lumps are highly distorted structures very close to further breakup. Hence, this liquid lumps are not regarded as droplets to be accounted for in the droplet concentration, the SMD nor the sphericity. First, α_l decreases over two orders of magnitude in the cavity. This is related to the acceleration of the liquid by the gas. Indeed, expressing the continuity of the liquid leads to $\alpha_l = \dot{m}_L/(\rho_l\overline{U}_L S)$ where $\dot{m}$ is the liquid mass flow rate and S the flow section of the cavity. The droplet concentration N_d increases continuously for z between 4 and 10 mm. This corresponds to the fragmentation of the jet which is the primary breakup. For $z > 10$ mm, the slope of $N_d(z)$ is lower, suggesting another mode of breakup, which could be secondary breakup in the present case. Concerning the SMD, the values for $z < 10$ mm are not representative due to the low number of droplets. For $z > 10$ mm, the decrease of the SMD illustrates the secondary breakup. The local maximum of

φ at z = 3 mm is due to small droplets torn directly at the nozzle orifice. They are due to the combination of a high shearing and too coarse spatial resolution. From the point of view of an experimentalist, the axial evolution of the sphericity is interesting because it gives an indication where the droplets are almost spherical, and therefore where PDA technique could be successfully applied. In the present case, at the outlet of the domain φ is close to an asymptote, which gives information on the steady state of the spray. This will be discussed later in terms of breakup events. The local maximum at z $\approx$ 3 mm corresponds to small droplets torn from the jet directly at the nozzle exit. This might be explained by a too coarse resolution.

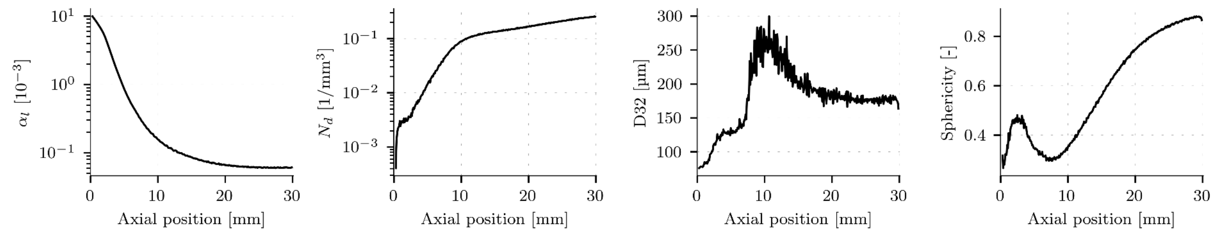

Figure 7 Axial evolution of the liquid fraction, number of droplets, SMD and sphericity.

Spray characteristics

On the animations extracted from both the experiment and the simulation, strong periodical fluctuations of liquid density were observed, as highlighted in Fig. 8. This is caused by the super pulsating mode of the liquid jet that was identified previously by Farago & Chigier [14]. Please note that the super pulsating mode occurs at high Weber and Reynolds numbers, in the fiber-type breakup regime. Therefore, it is not related to the flapping instability. The time series of the droplet concentration, the volume fraction and the liquid mass flow rate $\dot{m}$ were recorded at the outlet of the domain (slice 2 in Fig. 5) in order to identify the super pulsating mode. They are shown in Fig. 9. A variation of more than 100% a observed for the three quantities aforementioned. A Fourier Transform was applied, and the resulting cross spectra were improved using windowing and zero padding.

Figure 8 Illustration of the high periodical change between low and high-density regions.

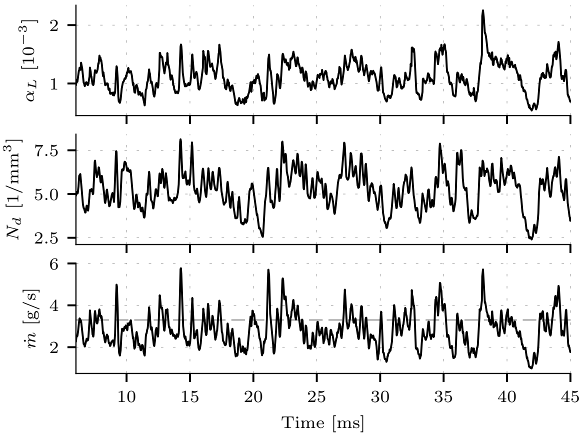

Figure 9 Temporal signal of α_L, N_d and $\dot{m}$ at the exit of the domain (slice 2).The dashed grey line is the prescribed liquid mass flow rate.

The Cross Spectrum Density (CSD) between the signals of α_l and N_d is presented in Fig. 10. A peak at 182 Hz is detected, which could be a suitable candidate for the frequency of the super-pulsating mode.

The spray characteristics, namely the velocity and the drop size distribution, were calculated for the two slices presented in Fig. 5. The axial and radial components of the velocity are plotted versus the radial coordinate in Fig. 11. The maximum axial droplet velocity (Fig. 11 left) is reached at the centerline, due to (i) the opening of the turbulent high speed air stream and (ii) the turbulence induced the intermittent flapping of the liquid jet. In the early stage of the breakup (slice 1), the profile of the axial velocity shows different plateaus, which are smoothed out at the outlet (slice 2) due to turbulent dispersion of the liquid phase. The radial velocity of the droplets (Fig. 11 right) is one order of magnitude lower that the axial velocity and decreases at larger z. On slice 1, the radial velocity is high because of the intermittent flapping events. On slice 2, the radial velocity is decreased due to friction and diffusion of momentum.

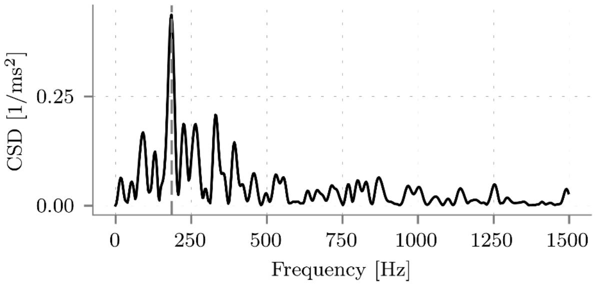

Figure 10 CSD of the volume fraction and the droplet concentration for z>25 mm.

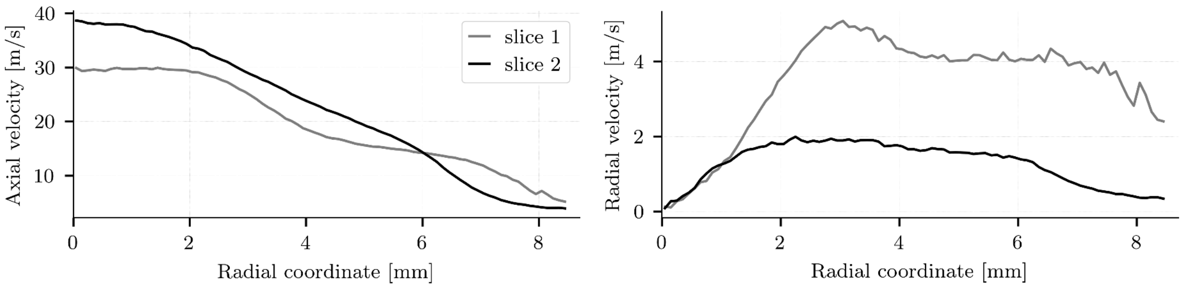

Figure 11 Radial profiles of the liquiq axial (left) and radial (right) velocity.

The volume drop size distribution within the two slices is presented in Fig. 12, superimposed with the SMD as dashed vertical line. The dotted line corresponds to best fit of a Rosin-Rammler function whose peaks are located at 46 and 44 µm for slice 1 and 2, respectively. The characteristics of the spray evolve from a SMD of 234 µm and a maximum diameter of 1.4 mm within slice 1, to a SMD of 144 µm and a maximum diameter of 0.9 mm within slice 2. It is observed that the shape of the PDF resolved by the numerical simulation is truncated at the lower diameters range, which compromises the determination of the peak value of the PDF. This is due to the too coarse spatial resolution, which requires to discard the small diameters from 0 to 66 µm. Nevertheless, the fitting of the data with the Rosin-Rammler distribution in Fig. 12 shows that the resolved scales of the droplet size ca be represented by this type of distribution, which is a promising result. In addition, the fitting allows to picture the shape of the distribution, and especially, the increase of the peak on slice 2, which illustrates the homogeneization of the spray. Please note that the same configuration was simulated in 2D [9] with a particle size of 20 µm and the peak was resolved. This suggests that in the present 3D case, a slight decrease of the particle size from 33.33 µm to 20 µm might resolve the peak of the PDF.

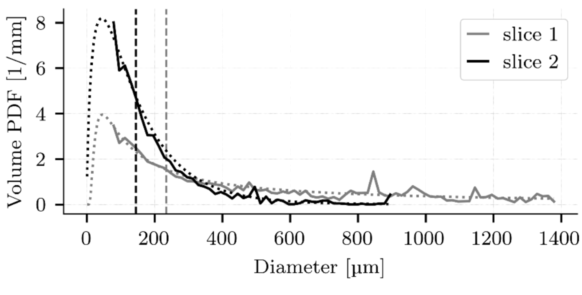

Figure 12 Droplet size volume distribution at the early stage of the breakup (grey) and at the domain outlet (black)

Fragmentation tree

Finally, due to the Lagrangian nature of the SPH method, it is possible to build the tree of fragmentation from the set of the particle clusters. The tree of fragmentation is defined here as a chained object that contains all the relationships between fragmented droplets, as illustrated in Fig. 13. This tree of fragmentation enables to extract various quantities like the number of breakup events that a droplet undergoes before exiting the domain, or the distribution of the d_{child}/d_{mother} ratio, also referred to as the *fragmentation intensity spectrum* [15]. The position $\mathbf{r}_{bu}$ of the breakup event is defined as the mass-weighted barycentric mean position of the mother drop and the

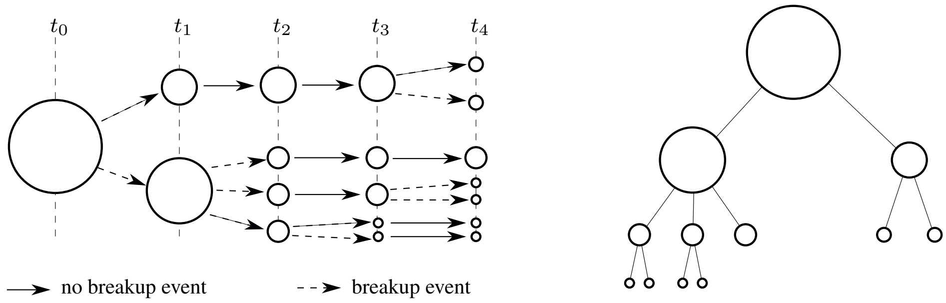

Figure 13 Time evolution of the breakup of a single droplet (left) and its corresponding tree of fragmentation (right).

child droplets:

$$\mathbf{r}_{bu} = \frac{(m\,\mathbf{r})_{\text{mother}} + \sum\limits_{\text{children}} m\,\mathbf{r}}{m_{\text{mother}} + \sum\limits_{\text{children}} m} \tag{5}$$

The time of breakup event t_{bu} is given by the last time of the mother drop and the first time of the child droplet. For instance, considering the breakup events between t_0 and t_1 on Fig. 13, the time t_{bu} of the breakup event is $t_{bu} = (t_0 + t_1)/2$. By projecting all breakup events on a background grid, it is possible to define the *breakup activity* N_ϕ, defined here as the number of breakup event per volume and per unit time. Figure 14 shows the axial and radial profiles of the breakup activity N_ϕ. The axial evolution of N_ϕ shows that the maximum of the breakup activity occurs at z $\approx$ 11 mm, which corresponds to the mean intact length of the liquid jet. At the outlet of the domain, N_ϕ goes to zero, suggesting that the spray is in a stable form, *i.e.* its drop size distribution will not change anymore. With regards to industrial applications, this is a valuable information for predicting where the spray has reached its steady drop size distribution. The radial profile of N_ϕ shows that the most active region is 0.5< r <1 mm, which is the location of the prolongation of the liquid duct. It is an unexpected results because one might expect that most of the breakup events would occur within the vorticity thickness of the air stream, initially located a r >1 mm.

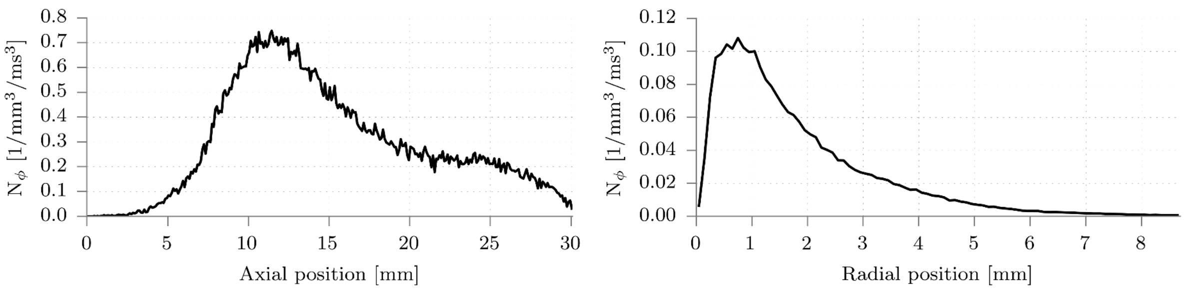

Figure 14 Axial (left) and radial (right) profiles of the number of breakup events per volume and time unit

In the following, the distribution of $q = d_c/d_m$, the ratio of the child droplet diameter d_c to the mother droplet diameter d_m is investigated. The statistical distribution of q is presented in Fig. 15 (left) in terms of Probability Density Function (PDF) and Cumulative Density Function (CDF). The values have been determined for the whole domain. The dashed line corresponds to $q = 1$ and marks the limit between breakup and coalescence. According to the CDF, 83.4% of the events are of breakup type. On the PDF, the two different phenomena can be discriminated by two different slopes in the log-log plot. However, the sharp change of slope occurs at $q \approx 1.2$ and not at q = 1. Note that the region $1 < q \leq 1.2$ contains most of the coalescence events. A maximum in the PDF is located at q $\approx$3 $\times$ 10^{-4}. This very low value of q indicates a breakup by peeling off large liquid structures. It can not be stated if this maximum corresponds to physics or if it is a numerical artifact due to the limited spatial resolution. Large values of q (>5) represent a droplet impacting a much large liquid lump, and could be labeled *impaction* instead of *coalescence*.

The same analysis is applied to the statistical set limited by $q < 1$ and plotted in Fig. 15 (right). It is labeled *fragmentation intensity spectrum* by Gorokhovski & Saveliev [15]. The region q <10^{-4} is not commented due to the lack of confidence in the spatial resolution. For q >10^{-3}, the PDF is piecewise linear. This linear curve in the log-log plot corresponds to a fragmentation spectrum as a power law, which is typical for a fragmentation spectrum [16].

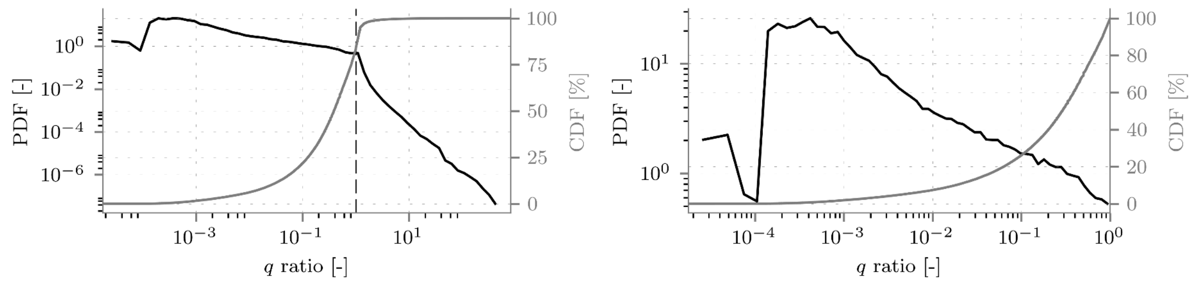

Figure 15 Distribution of $q = d_c/d_m$ (left) and fragmentation intensity spectrum (right).

The number of breakup events $N_{bu/drop}$ that a droplet undergoes before leaving the domain is plotted in Fig. 16 (left) as probability density and cumulative sum. It is found that 72% of the droplets leaving the domain do not undergo any breakup event after the initial peeling off from the jet. The linear decrease of the histogram plot suggests a probability density function of the number of breakup event in the form $f_{N_{bu/drop}} \propto \mathrm{e}^{-a\, N_{bu/drop}}$ where a is a positive constant. The reciprocal quantity of $N_{bu/drop}$, namely the number of droplets generated in a single breakup event $N_{drop/bu}$, is plotted in Fig. 16 (right). More than 75% of breakup events generate two child droplets, while approx. 15% generate three droplets. The hyperbole shape of the histogram suggest a distribution of $N_{drop/bu}$ in the form $f_{N_{drop/bu}} \propto \mathrm{e}^{a/N_{drop/bu}}$.

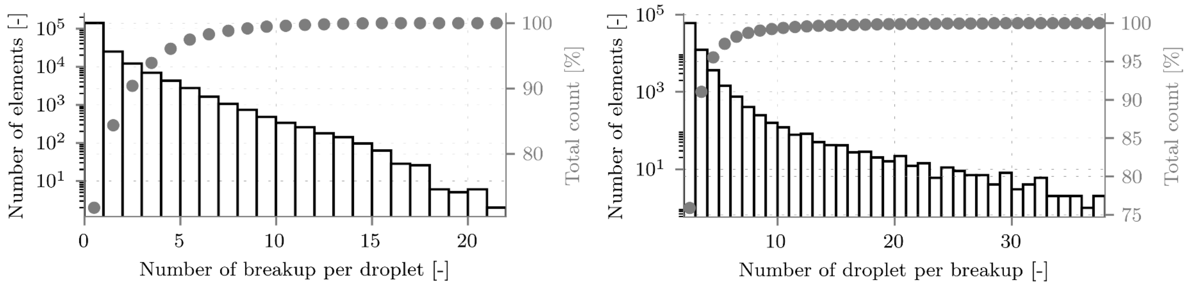

Figure 16 Number of breakup event per droplet (left) and number of droplet per breakup event (right)

Conclusion

In this work the air-assisted disintegration of a viscous liquid jet at high ambient pressure was simulated by means of the SPH method, and compared to experimental investigtions. Comparison to high-speed images from the experiment shows that agreement is good both in terms of spatial and temporal evolution. Projecting axial profiles of the spray characteristics illustrated the establishment of the steady state of the spray. The super pulsating mode, observed in both the simulation and the experiment, was quantitatively measured in terms of temporal evolution and its frequency was estimated for the first time. Extracting the spray quantities within two different slices located downstream the nozzle allowed to anayze the homogenization of the spray, in terms of (i) kinematics (velocity profiles) and of (ii) granulometry (size distribution). However, the spatial resolution of 33.33 µm used for the simulation is too coarse to resolve the whole drop size PDF. The breakup activity was plotted versus the radial and axial coordinate. It was found that the spray was almost stable at the outlet of the domain. In the pure breakup regime ($q < 1$), the fragmentation intensity spectrum is well described by a power law, according to previous theoretical developments.

In summary, the SPH method showed strong advantages for predicting air-assisted atomization and for capturing the whole breakup cascade, from primary instabilities to the spray characteristics. For the first time, the full breakup cascade was investigated with the aid of the tree of fragmentation.

Acknowledgement

The authors like to thank the Helmholtz Association of German Research Centres (HGF) for funding (Grant No. 34.14.02). This work was performed on the computational resource ForHLR Phase I funded by the Ministry of Science, Research and the Arts Baden-Württemberg and DFG ("Deutsche Forschungsgemeinschaft"). The authors also like to thank Harmut Häfner from KIT-SCC for technical support on the HPC cluster.

References

[1] Dahmen, N.; Dinjus, E.; Kolb, T.; Arnold, U.; Leibold, H. and Stahl, R., *Environmental Progress & Sustainable Energy*, 31(2):176–181 (2012).

[2] Jakobs, T.; Djordjevic, N.; Fleck, S.; Mancini, M.; Weber, R. and Kolb, T., *Applied energy*, 93:449–456 (2012).

[3] Li, X. and Soteriou, M. C., *International Journal of Multiphase Flow* (2018).

[4] Behzad, M.; Ashgriz, N. and Karney, B., *International Journal of Multiphase Flow*, 80:100 – 117 (2016).

[5] Müller, T.; Sänger, A.; Habisreuther, P.; Jakobs, T.; Trimis, D.; Kolb, T. and Zarzalis, N., *International Journal of Multiphase Flow*, 87:212 – 228 (2016).

[6] Monaghan, J. J., *Reports on Progress in Physics*, 68:1703 – 1759 (2005).

[7] Höfler, C.; Braun, S.; Koch, R. and Bauer, H.-J., *J. Eng. Gas Turbines Power*, 135:1 – 8 (2013).

[8] Koch, R.; Braun, S.; Wieth, L.; Chaussonnet, G.; Dauch, T. and Bauer, H.-J., *European Journal of Mechanics - B/Fluids*, 61(Part 2):271 – 278 (2017), rotating Flows.

[9] Chaussonnet, G.; Koch, R.; Bauer, H.-J.; Sänger, A.; Jakobs, T. and Kolb, T., *Journal of Fluids Engineering*, 140(6):061301 (2018).

[10] Jakobs, T.; Djordjevic, N.; Sanger, A.; Zarzalis, N. and Kolb, T., *Atomization and Sprays*, 25(12) (2015).

[11] Sänger, A.; Jakobs, T.; Djordjevic, N. and Kolb, T., *Proceedings of the Triennal International Conference on Liquid Atomization and Spray System (ILASS)* (2015).

[12] Hussein, H. J.; Capp, S. P. and George, W. K., *Journal of Fluid Mechanics*, 258:31–75 (1994).

[13] Rosenfeld, A. and Pfaltz, J. L., *Journal of the ACM (JACM)*, 13(4):471–494 (1966).

[14] Farago, Z. and Chigier, N., *Atomization and Sprays*, 2:137–153 (1992).

[15] Gorokhovski, M. and Saveliev, V., *Journal of Physics D: Applied Physics*, 41(8):085405 (2008).

[16] Brown, W. K., *Journal of Astrophysics and Astronomy*, 10(1):89–112 (1989).